Dual-Band Circularly Polarized Antenna Array for 5G Millimeter-Wave Applications

SAMANEH SADEGHI-MARASHT [1] (Student Member, IEEE),
MOHAMMAD S. SHARAWI [2] (Senior Member, IEEE), AND **ANDING ZHU** [1] (Fellow, IEEE)

[1] School of Electrical and Electronic Engineering, University College Dublin, Dublin 4, D04 V1W8, Ireland

[2] Department of Electrical Engineering, Polytechnique Montreal, Montreal, QC H3T 1J4, Canada

CORRESPONDING AUTHOR: S. SADEGHI-MARASHT (e-mail: samaneh.sadeghimarasht@ucdconnect.ie)

ABSTRACT A dual-band miniaturized e-shaped antenna with circular polarization (CP) at 28 and 38 GHz is presented in this work for 5G millimeter-wave applications. Characteristic mode analysis (CMA) is used in the design steps of the antenna. This compact antenna consists of a main radiating patch surrounded by an L-shaped and hat-shaped metallic strips. The design was implemented on a single RO5880 substrate with a thickness of 0.508 mm, and fed by a single coaxial cable. A 2×2 antenna array was also developed and validated. The dimensions of this array were $1.5 \lambda_0 \times 1.86 \lambda_0$ (where λ_0 is the free space wavelength at 28 GHz). In the lower band of 28 GHz, 95% total efficiency and 12.69 dBiC gain were obtained, while in the higher band of 38 GHz, 90% total efficiency and 11.10 dBiC gain were achieved. The beamforming capability of this dual band array was investigated as well.

INDEX TERMS Beamforming, circular polarization, dual-band, high efficiency, patch antenna, single layer antenna array.

I. INTRODUCTION

TO MEET the demand for high capacity with high data rates, fifth generation (5G) wireless networks employ millimeter-wave (mm-wave) frequency bands and multiple-input multiple-output (MIMO) technology. The short wavelength at mm-wave frequencies leads to a smaller size of antenna, which means that antenna arrays with a larger number of elements can be fitted in a small space to provide a high gain to tackle the path loss at mm-wave frequencies [1], [2]. Another advantage of the array structure is that beamforming can be utilized to steer waves in the desired directions. The capacity and coverage of 5G cells can be enhanced by employing beamforming and MIMO, according to [3].

At mm-wave frequencies, circular polarization (CP) can be used to strengthen signal power and decrease delay [4]. CP can be accomplished by the use of a single or dual feed approach [5]–[7]. The dual feed antenna requires more space and has a complicated feeding design, making manufacture challenging. Several research on multi-band CP antennas

have been reported in [8]–[10], with the results obtained by employing multiple layers or various feeding arrangements. The CP antennas introduced in [11]–[13] had a limited axial ratio bandwidth (ARBW), however, the antenna in [14] had a broad ARBW but a low gain. Reference [15] studied a structure with and without a U slot and concluded that a U slot shape would result in a narrower ARBW. Other structures with fewer complications were presented in [16] and [17]. However, as illustrated in [17], these structures were quite massive, with 93 mm in length. Another approach for achieving CP with a broad bandwidth was suggested in [18], in which a partially reflecting surface (PRS) was employed at the antenna's top, however the required thickness made this design quite bulky.

In [19] it was proposed to use a single-layer CP patch antenna surrounded by a metasurface. The 2×2 antenna array was also designed using this single element, with a dimension of 20.4×20.4 mm² and a low diversity gain. Until recently, the majority of CP antennas were published as single band designs. Notably, a few multi-band antennas have
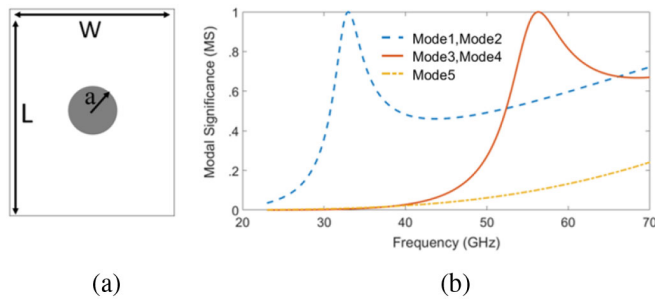
FIGURE 1. (a) Simple circular patch structure with a = 1.57 mm, W = 11 mm, L = 14 mm, and ϵ_r = 2.2, (b) MS of the circular patch.

FIGURE 2. Modes current of circular patch at 28 GHz, (a) mode 1, (b) mode 2, (c) mode 3, and (d) mode 4.

been developed, however they have a low gain or a limited ARBW [11], [22], [23].

This paper investigates a dual-band antenna array with circular polarization (CP) at each band, in which the patch shape is the major source of polarization rather than several layers or feedings. The proposed patch antenna was designed utilizing the characteristic mode analysis (CMA) technique. The CMA was used to analyze the generated modes at each frequency and to demonstrate how they can provide the CP. The results indicate that the antenna is not only low profile and capable of CP operating in the 28 GHz and 38 GHz frequency bands, but also has a relatively high gain and efficiency. Notably, several existing antennas have the CP with sophisticated feeding, multi-layer configurations, or lower gain than our design. A 2×2 array with a high gain and efficiency is constructed of this single element antenna covering the 5G mm-wave bands at 28 and 38 GHz with an ARBW of 3.2% and 1.65%, respectively. The array has an overall size of 17 × 20 mm^2 and each patch is fed through a simple coax cable.

II. CONFIGURATION OF THE DESIGNED ANTENNA
A. DESIGN OF ANTENNA ELEMENT
To design a dual-band single layer antenna operating at 28 GHz and 38 GHz, the radius of the circular patch is first calculated in relation to the frequencies at which the antenna will operate. The relation between frequency and the radius of a circular patch can be derived from [20]:

$$f_{mn} = \frac{X_{mn}c}{2\pi \sqrt{\epsilon_r}(a)} \tag{1}$$

where c denotes the speed of light, a denotes the radius of a circular patch, and X_{mn} denotes the nth root of the first kind Bessel function J_m of order m. The resonant frequencies are ordered as follows: f_{11}, f_{21}, f_{01} and so on. According to the values for X_{mn}, the resonant frequencies are f_{11} = 37.63 GHz, f_{21} = 62.24 GHz, and f_{01} = 78.57 GHz for a circular patch with radius of 1.57 mm designed on the substrate with permittivity of ϵ_r = 2.2 and thickness of 0.508 mm. The design and analysis steps of this work are carried out using the software CST Microwave Studio.

The characteristic mode analysis (CMA) technique is utilized in this paper to study the antenna's modal behavior
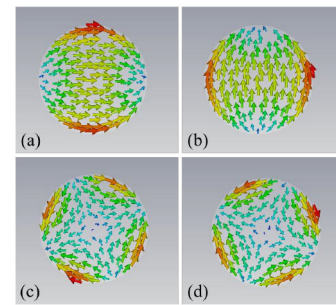
in order to design a dual-band CP patch antenna with only one layer and one feeding. As a result, the need for multi-layer or multi-feeding systems to achieve these goals will be eliminated. The structure is depicted in Fig. 1 (a), although it should be noted that the substrate material is not lossy in this method, and the circular patch is constructed of PEC with a thickness of zero. In Fig. 1 (b), the calculated modal significance curves are shown, with modes 1 and 3 overlapping with modes 2 and 4, respectively. These overlapping modes can be considered degenerated modes, however only modes 1 and 2 have orthogonal surface currents, as illustrated in Fig. 2.

The following step is to optimize the circular patch using modes 1 and 2. The optimized shape of the proposed radiating patch is shown in Fig. 3 (a), where the radiated E fields are not degraded and the two previously mentioned modes are also separated to create the CP feature. In Fig. 3 (b), modes 1 and 2 are separated, with their high modal significance (MS) at frequencies of 28 and 39 GHz. To achieve CP, additional modes with a high MS at our desired frequencies must be added to this structure. The characteristic angle curves for these two modes are shown in Fig. 3 (c), indicating that they are radiating modes at 29 and 39 GHz, respectively, as they cross the 180 degree at the desired frequencies. The other modes are either inductive (with a characteristic angle of < 180°) or capacitive (with a characteristic angle of > 180°) and do not cross with 180°.

B. CIRCULAR POLARIZATION AT 28 GHZ
The modified circular patch's modal currents are illustrated in Fig. 3 (d). A frequency of 38 GHz is associated with mode 1, while a frequency of 28 GHz is associated with mode 2. To obtain a clear view of high magnitude modes between 28 and 38 GHz, we set the reference frequency for defining the modes in CMA to a value greater than 38 GHz and use this value to decide the order of the modes. Fig. 3 (e) illustrates the radiated farfield patterns. According to the farfield directions of modes 1 and 2, the required mode for CP at the lower band (28 GHz) must be orthogonal to the direction of farfield radiation of mode 2, as illustrated in this figure, while another mode is required for 38 GHz to be orthogonal to the direction of mode 1. These modes will be
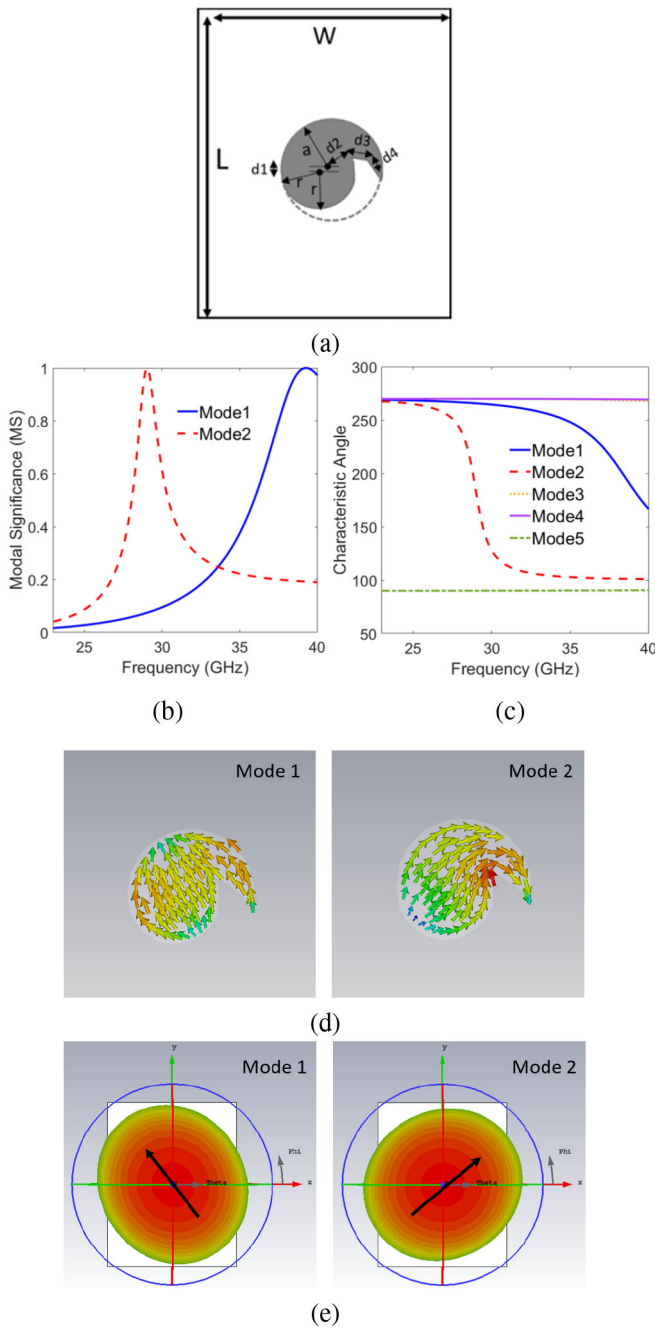
(a)

(b)

(c)

(d)

(e)

FIGURE 3. The configuration of separating modes, (a) modified circular patch with dimensions of W=11, L=14, a=1.57, r=1.15, d1=0.1, d2=0.7, d3=0.47 and d4=0.75 (all dimensions are in mm), (b) MS of modified circular patch, (c) characteristic angle of modified circular patch that shows radiation properties at 29 GHz and 39 GHz as the modes pass 180 degree at mentioned frequencies, (d) modal currents of mode 1 (for 38 GHz) and mode2 (for 28 GHz), (e) far-field radiation of mode 1 and mode 2.

(a)

(b)

(c)

(d)

(e)

FIGURE 4. The configuration of CP structure at lower band, (a) added L-shaped wall with dimensions of c3=3.12 mm and c4=4.7 mm, (b) modes of the structure with L-shaped wall, mode 1 is generated by this wall, (c) characteristic angle of mode 2 and added mode (mode 1), (d) the impact of c3 on modes 1 and 2, and (e) the impact of c4 on modes 1 and 2.

created by implementing specific conductive shapes close to the modified radiating patch. This position is selected based on the fact that all generated modes can be excited with just one coaxial feed connected to the modified circular patch. The lower band's added mode is created by employing the L-shaped wall shown in Fig. 4 (a). After optimizing the L-shaped wall, a similar MS is obtained for two orthogonal
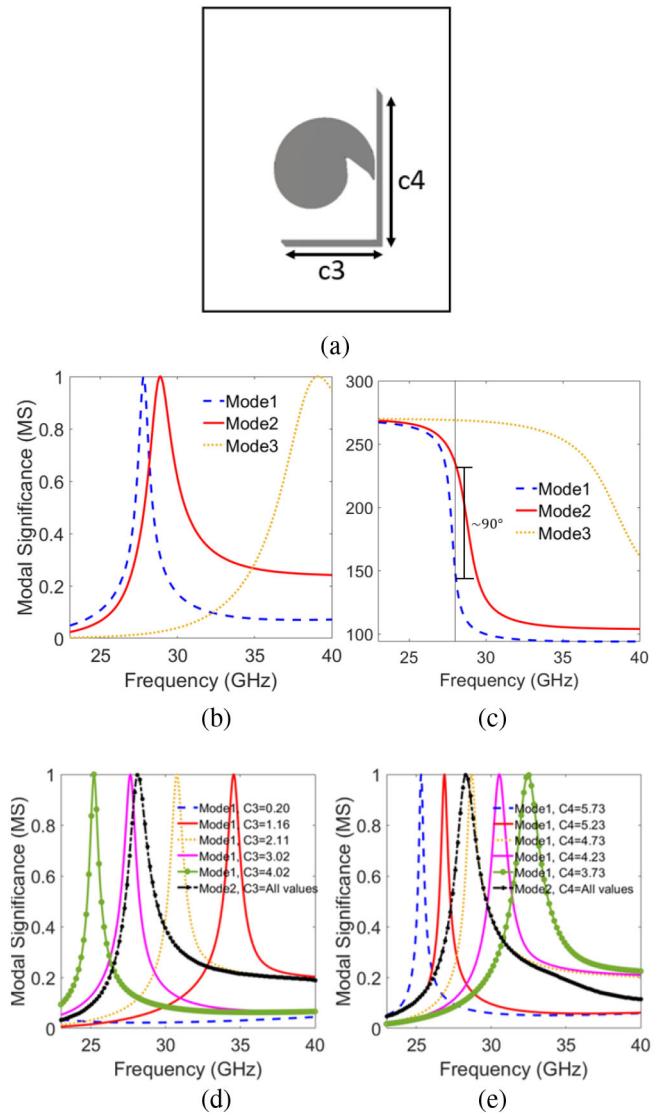
modes operating at 28 GHz. The idea behind this design is that the L-shaped conductor can be used to control the direction of the total current. The MS curve of the added wall is depicted in Fig. 4 (b). Note that, when modes are added to the structure, depending on the frequency defined in the software, the order of modes will be changed. Thus, at 28 GHz, the two modes are denoted as modes 1 and 2. The added mode generated by the L-shaped wall is nearly identical to mode 2 at 28 GHz, and the phase difference between these two modes is nearly 90 degrees, as indicated in Fig. 4 (c). Fig. 4 (d) and Fig. 4 (e) illustrate the effects of the parameters c_3 and c_4 on mode 1. Due to the lack of significant effects on modes 2 and 3, the curves for these modes are not shown. The optimal values for these parameters can be determined by considering the situations in which mode 1
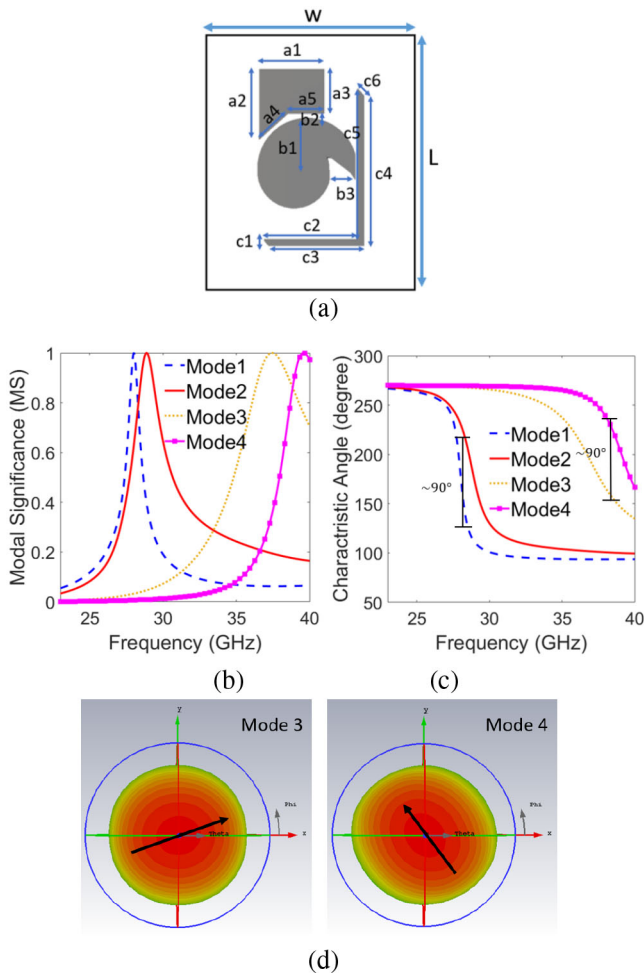
(a)

(b)

(c)

(d)

FIGURE 5. The configuration of dual-band and CP structure, (a) final designed antenna with dimensions of a1=2.05, a2=2.2, a3=1.4, a4=1.20, a5=1.15, b1=1.57, b2=0.13, b3=0.82, c1=0.20, c2=2.94, c3=3.12, c4=4.7, c5=4.73, c6=0.41, W=11 and L=14 (all dimensions are in mm), (b) four generated modes of the final structure, (c) characteristic angle of all the modes, and (d) the far-field radiation of mode 3 and mode 4 that are orthogonal to each other at 38 GHz.

meets mode 2 with a high magnitude. In this design, the values of 3.12 mm for c3 and 4.7 mm for c4 were selected.

C. CIRCULAR POLARIZATION AT 38 GHZ

Another mode must be added to the structure that has the same MS as mode 3 at 38 GHz, and a phase difference of 90 degrees must be maintained between them to obtain CP. A radiating part similar to the L-shaped component that operated at 28 GHz was designed. However, the reflection coefficient and CP results were not satisfied simultaneously because the MS of the created modes at 38 GHz were not sufficiently high, resulting in an mismatched reflection coefficient. This is why the shape utilized at the lower frequency cannot be used at the higher one. Following multiple parameter optimizations and an investigation of several shapes, the final structure seen in Fig. 5 (a) was designed. At 38 GHz, the generated mode 4 is orthogonal to mode 3. CMA analysis of this structure shows two modes with almost identical values at 38 GHz and a phase difference of about 90 degrees,
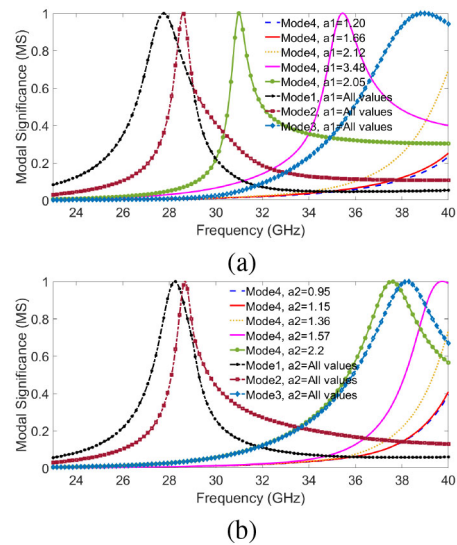

(a)

FIGURE 6. The impact of different values of (a) a1 on modes 1-4, and (b) a2 on modes 1-4 for the final designed structure of single element antenna.
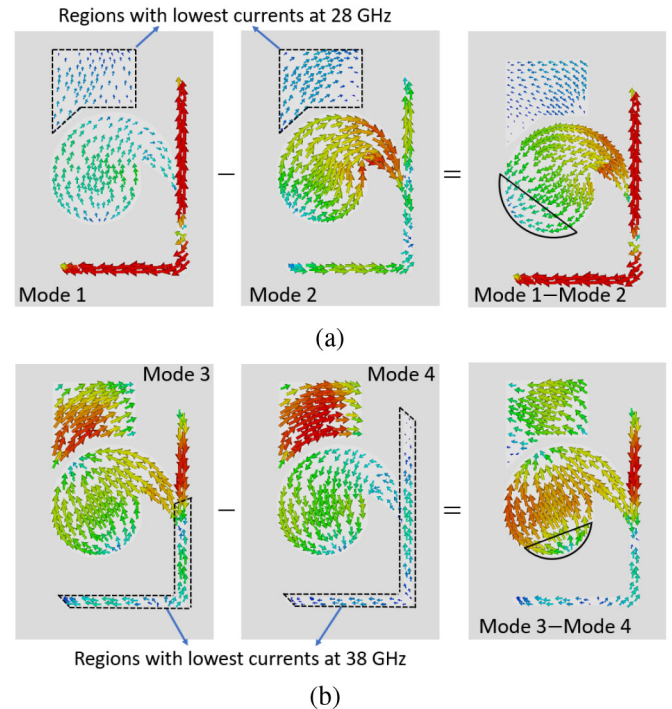

(a)

(b)

FIGURE 7. Surface currents of (a) mode 1, mode 2 and difference between them at 28 GHz, (b) mode 3, mode 4 and difference between them at 38 GHz.

as illustrated in Figs. 5 (b) and (c). The farfield generated by modes 3 and 4 is depicted in Fig. 5 (d). This conductor has been optimized for the purpose of moving the new added mode with a high MS to the main mode at 38 GHz. The optimization procedure for two important conductor parameters is shown in Fig. 6 (a) and Fig. 6 (b), which demonstrates that this conductor has the greatest influence on mode 4 and the least influence on the other modes (i.e., 1-3). Thus, the optimal values for these parameters can be selected so that
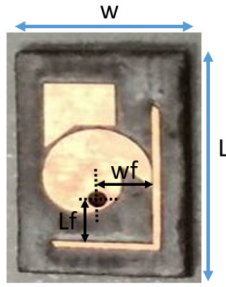
FIGURE 8. The fabricated single element antenna with dimensions of W=11, L=14, Wf=1.59 and Lf=1.45 (all dimensions are in mm).

the added mode and the main mode at 38 GHz overlap with a high magnitude and an almost 90 degree phase difference. As a result, the numbers 2.05 mm for a1 and 2.2 mm for a2 were selected.

## III. SINGLE ELEMENT *E*-SHAPED CP ANTENNA

The CMA analysis used in the previous section explains the physical geometry of the designed antenna that enables CP and dual band properties. Now the full-wave simulation is conducted using a simulated mini-smp connector as the feed. The feeding position is critical in getting the desired results, and it is optimized to excite all of the aforementioned modes (modes 1–4 in Fig. 5 (b)). Notably, if the feeding location is chosen in such a way that only a few of the aforementioned modes are activated with high magnitude, the CP or impedance matching is violated. The optimal location for feeding is where the currents of each mode have a high similar value. As shown in Fig. 7 (a), the regions with the lowest currents for both modes 1 and 2 are highlighted (top square patch), indicating that we will disregard them when determining the feeding location because we require higher mode currents; the remaining sections for both modes have a higher value, that must be considered for finding a similar high value.

This was accomplished by subtracting them from one another, as seen in the rightmost figure of Fig. 7 (a), where the lowest value is highlighted. For 38 GHz, the regions with the lowest current density are depicted in Fig. 7 (b) (on the L shape), and we will not consider them when estimating the feeding position because high current values are required. We subtracted the two as shown on the right side of Fig. 7 (b); the region with similar high value currents is shown in that figure. The feeding position can be predicted using the common location of both these subtracted sections at 28 GHz and 38 GHz. The final precise position of the feeding is determined by optimizing the estimated one in the full wave simulation while taking impedance matching and CP into account at both 28 and 38 GHz.
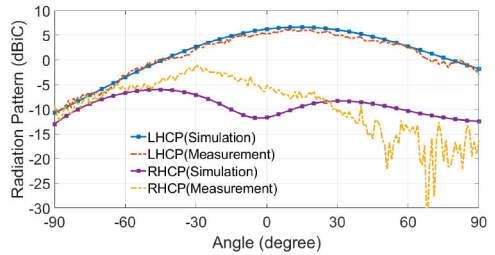
The BW of this structure was 5.05% at 27-28.4 GHz and 14.10% at 34.7-40 GHz for 28 GHz and 38 GHz, respectively. The fabricated version of the designed single element antenna in Fig. 5 (a) with the optimized feeding
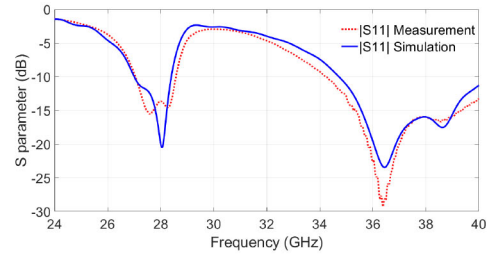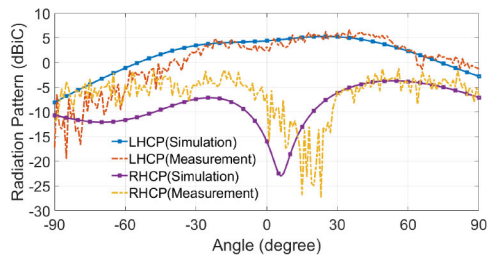

(a)
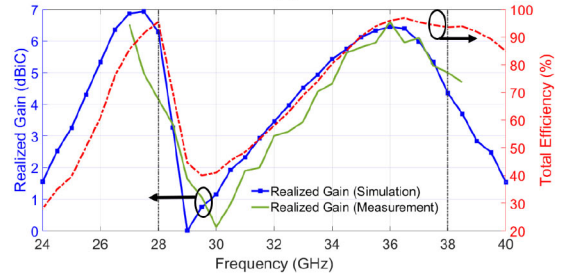
(b)

(c)

(d)

FIGURE 9. The obtained results of the designed dual band CP single element antenna, (a) the |S11| in full wave simulation which is illustrated by blue solid line and measurement is shown by dotted red line, (b) simulated and measured realized gain with simulated total efficiency over different frequencies, (c) simulated and measured radiation pattern at 28 GHz, and (d) simulated and measured radiation pattern at 38 GHz.

position is shown in Fig. 8. As seen in Fig. 9 (a), the measurement of the reflection coefficient closely follows the simulation. Fig. 9 (b) shows the high efficiency of 93% for both frequencies of 28 GHz and 38 GHz, with achieved gains of 6.26 dBiC and 4.32 dBiC, respectively. The simulation closely matches the measured realized gain. Furthermore, the proposed antenna's high efficiency is due to the low dielectric constant and low loss of the rogers "RO5880" material utilized as the substrate, as well as the well impedance matching of the designed antenna, especially at 28 GHz. This antenna has left-handed circular polarization (LHCP)
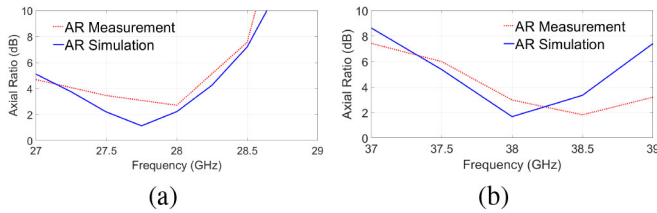
FIGURE 10. Axial Ratio over frequency of single element antenna that is below 3 dB for (a) lower band of 28 GHz and (b) higher band of 38GHz.
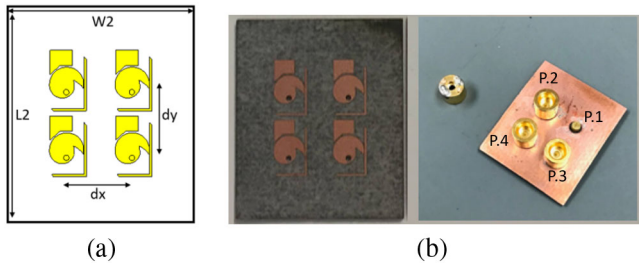

FIGURE 11. The structure of 2 × 2 antenna array with dimensions of W2=17 mm, L2=20 mm, and center to center space between elements of dx = dy = 6 mm, (b) front view and back view of the fabricated 2 × 2 antenna array with the ports label.

TABLE 1. Comparison of different distances between patches of array.

Freq.	28 GHz			38 GHz		
Dist. (dx=dy)	5(mm)	6(mm)	7(mm)	5(mm)	6(mm)	7(mm)
Gain(dBiC)	12.1	12.8	13.8	11.8	11.5	10.1
SLL(dB)	-29.1	-23	-15.3	-12.4	-6.8	-2.4
AR(dB)	3.7	2.1	2.4	2	0.9	2.2

With these optimized distance values, the coupling between elements is low, and the magnitude of the reflection coefficient for each port of this antenna array is less than −10 dB at the desired frequencies of 28 GHz and 38 GHz, respectively. The effect of varying the distance between antenna array patches is shown in Table 1, demonstrating that the best results for both bands are obtained at a 6 mm (0.56 λ_0) center to center distance between patches in both x and y directions. The CP of the lower band will deteriorate over a shorter distance, while the SLL of the higher band will deteriorate over a longer distance.

The measured and simulated reflection coefficients of the array are shown in Fig. 12 (a) for ports 1 and 2, and their mutual coupling is shown in Fig. 12 (b). Figs. 12 (c) and (d) illustrate the achieved reflection coefficient and mutual coupling values for ports 3 and 4, respectively. Mutual coupling is less than −20 dB for all indicated ports, with an operational BW of 5.6% at 28 GHz and 18.42% at 38 GHz. The simulated mutual coupling was less than −15 dB for $|S13|$, $|S14|$, $|S23|$, and $|S24|$. Additionally, Fig. 13 illustrates the magnitude of the array's reflection coefficient when all ports are activated simultaneously. The reflection coefficient is less than −10 dB at both 28 GHz and 38 GHz operating frequencies, as illustrated.

This antenna array has CP properties, as the AR of this structure is below 3 dB at the desired frequencies. The AR of this array's port 1 is determined by connecting it to the measurement system while the remaining ports are connected to the matching loads. As illustrated in Fig. 14 (a), the simulated and measured AR for port 1 at 28 GHz is 0.93 dB with a 4.1% ARBW and 1.2 dB with a 3.07% ARBW. At 38 GHz, these values are 2.37 dB with a 2.5% ARBW and 1.1 dB with a 2.44% ARBW, respectively, as shown in Fig. 14 (b). The simulated AR for the antenna array when all ports are excited is available in Fig. 15 (a) for 28 GHz with 2.1 dB and 3.2% ARBW, and in Fig. 15 (b) for 38 GHz with 0.9 dB and 1.65% ARBW.

The single element maximum gain was at least 6.98 dBiC for the elements within the array. Maximum realized gain of 12.69 dBiC and 11.1 dBiC were achieved for the 28 GHz and 38 GHz bands, respectively. The efficiencies in the two bands were 92% and 91%, respectively. The gain and efficiency curves versus frequency are shown in Fig. 16 (a). The obtained realized gain is very close to the simulated value. As discussed for the single element, this designed antenna array has LHCP, and the proposed antenna array's simulated and measured radiation patterns are shown in Fig. 16 (b) and (c) for 28 GHz and 38 GHz, respectively. As illustrated in

as the main beam direction illustrated in Figs. 9 (c) and (d) are LHCP for 28 GHz and 38 GHz, respectively. The measurement agrees closely with the simulation, as demonstrated in these figures. Interestingly, by using the mirror shape of the proposed radiating patch to reverse the provided currents, this polarization can be changed to RH.

At 28 GHz, the simulated and measured AR of a single element antenna were 2.2 dB and 2.7 dB, respectively, as shown in Fig. 10 (a). Likewise, for 38 GHz, these values were 1.66 and 2.9, as shown in Fig. 10 (b). The fact that these values for the two frequencies are less than 3 dB indicates that the radiating wave has CP characteristics in the boresight direction. For 28 GHz, the simulated and measured ARBW were 2.5% and 0.8%, respectively, and 1.5% and 5% for 38 GHz. The difference between the simulated and measured results can be attributed to measurement setup errors as well as manual soldering of the mini-smp connectors.

IV. 2×2 ANTENNA ARRAY WITH DUAL-BAND CP

The total E-field of the antenna array can be calculated using pattern multiplication method [21]. Additionally, an interesting feature of the array structure is its capacity to do beamforming in any direction. The phase required between elements can be changed as described in [20] in order to steer the beam. Fig. 11 (a) shows the antenna array, which is constructed of four designed single elements, with an optimal center to center distance of 0.56 λ_0 (where λ_0 is the free space wavelength at 28 GHz) in both vertical and horizontal directions. The antenna array prototype with soldered mini-smp connectors is illustrated in Fig. 11 (b). Notably, the array's ground size is larger than that of a single element, yet the obtained results are independent of the ground size.
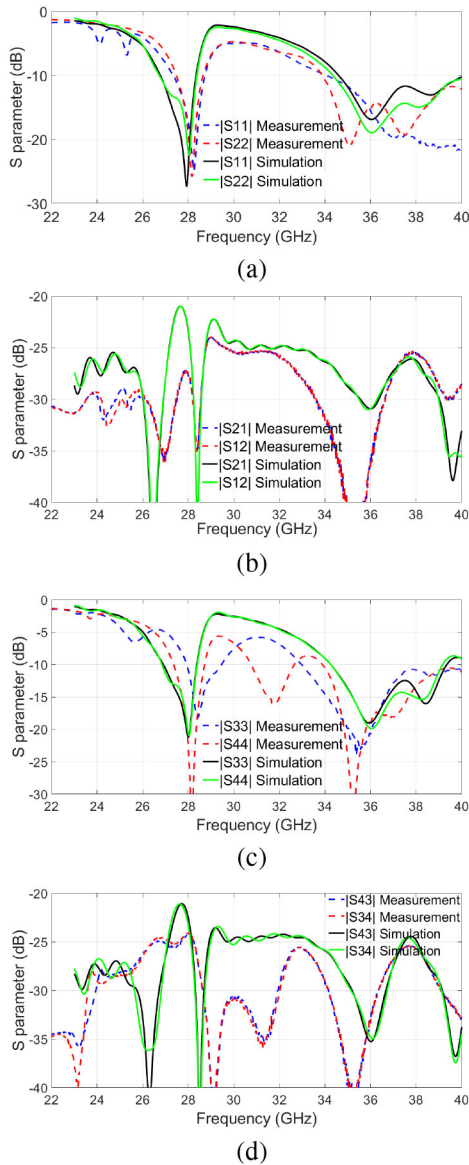
(a)

(b)

(c)

(d)

FIGURE 12. Measured and simulated magnitude of S-parameter of 2×2 antenna array for port 1 and port 2 (a) reflection coefficient, (b) mutual coupling, for port 3 and port 4 (c) reflection coefficient, (d) mutual coupling.
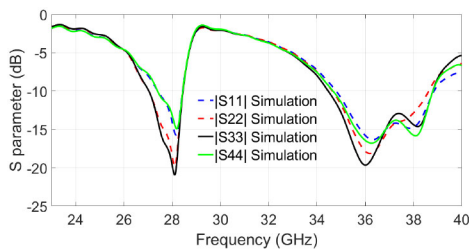

FIGURE 13. Simulated magnitude of S-parameter of 2×2 antenna array when all ports are activated.

these figures, the measurement and simulation are in perfect agreement.

The beamforming of this 2 × 2 antenna array is shown in Fig. 17 for $\phi = 0$ at 28 GHz and in Fig. 18 for 38 GHz.
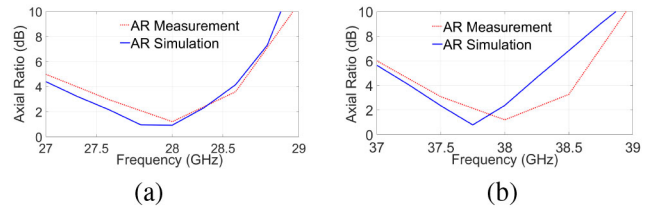

(a) (b)

FIGURE 14. Simulated and measured AR over frequency of 2 × 2 antenna array for port 1 that is below 3 dB for (a) lower band of 28 GHz and (b) higher band of 38GHz.

(a) (b)
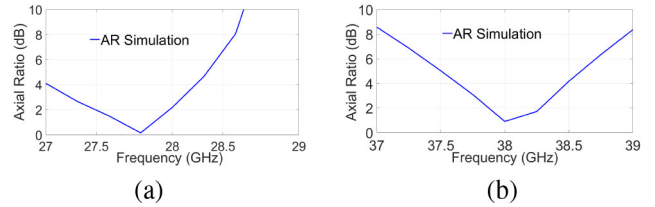
FIGURE 15. Simulated AR over frequency of 2 × 2 antenna array that is below 3 dB for (a) lower band of 28 GHz and (b) higher band of 38GHz.

(a)

(b)

(c)
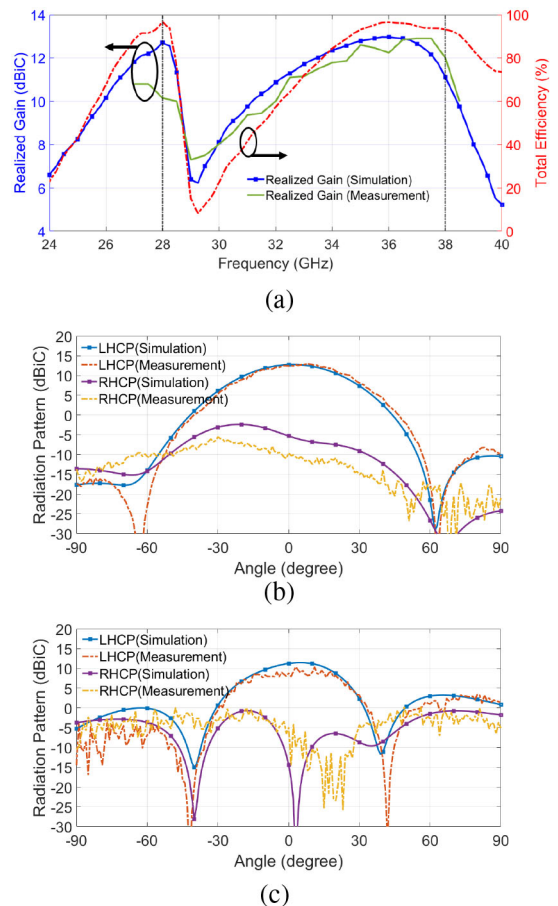
FIGURE 16. The obtained results of the designed dual band CP 2 × 2 antenna array, (a) simulated and measured realized gain with simulated total efficiency over different frequencies, (b) simulated and measured radiation pattern at 28 GHz, and (c) simulated and measured radiation pattern at 38 GHz.

The sidelobe levels are obtained for a 2 × 2 antenna array and can be reduced by increasing the number of elements in the array. By using the calculated progressive phase, as

TABLE 2. Comparison of the proposed mm-wave CP 2×2 antenna array with previous works.

Ref.	Dual/ Single band	Array/ Single Element	LP/ CP	Radi. Eff.(%)*	|S11| BW(%)	AR BW(%)	Size (λ_0)	Gain (dBiC)
[16]	Single	SE	CP	69&76	28.6	28.6	0.47×3.7×1.85	12
[17]	Single	SE	CP	NG	5	5.9	7.5×4.08×0.12	8.5
[18]	Single	SE	CP	NG	27.6	17	9.3×9.30×0.70	14.1
[19]	Single	SE	CP	95	23.4	16.8	1.0×1.0×0.04	11
[22]	Dual	SE	LP&CP	95&93	2.15&2.90	LP&2.65	0.74×0.74×0.02	6
[23]	Dual	SE	CP	88&90	5.25&10.5	NG	0.74×0.74×0.04	5.1&5.7
[11]	Dual	SE	CP	84&91	3&1.9	0.7&1.05	0.63×0.63×0.02	4&4.5
Prop.	**Dual**	**SE**	**CP**	**94&96**	**5.05&14.10**	**2.5&1.5**	**1.3×1.02×0.04**	**6.73&5.51**
[24]	Single	Array	LP	-	18.2	-	6×6×0.48	15.3
[25]	Single	Array	LP	92	7.14	-	2.8×2.8×0.07	6.1
[26]	Single	Array	CP	NG	25.86	NG	5.1×4.35×0.098	14
[27]	Single	Array	CP	84	25.7	17	2.7×2.7×0.28	15.1
[28]	Single	Array	CP	NG	33.8	5	5.2×2×0.15	9.5
[29]	Single	Array	CP	70	14.28	4.10	3.1×2.8×0.2	7
[30]	Single	Array	CP	84	15.6	10	1.6×1.6×0.11	13.5
Prop.	**Dual**	**Array**	**CP**	**94&94**	**5.6&18.42**	**3.2&1.65**	**1.5×1.86×0.04**	**12.69&11.1**

* Simulated radiation efficiencies are demonstrated in this column for all previous works.
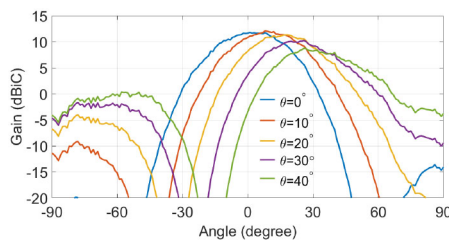

FIGURE 17. Measured beamforming of 2 × 2 antenna array at 28 GHz.
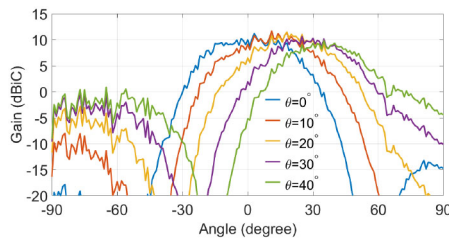

FIGURE 18. Measured beamforming of 2 × 2 antenna array at 38 GHz.

seen in 2, the beam can be tilted in the elevation direction:

$$\Delta\phi = \frac{2\pi d \sin\theta}{\lambda} \quad (2)$$

where θ represents the angle of the tilted beam, d is the distance between elements and λ represents the wavelength at 28 and 38 GHz, respectively. The maximum measured gain at 28 GHz is 11 dBiC, while the maximum measured gain at 38 GHz is 9.34 dBiC. At 28 GHz, the array's maximum tilt angle is $-29°$ to $32°$, while at 38 GHz, it is $-24°$ to $35°$. When the beam is tilted to 40 degrees for 28 GHz, the gain is reduced by 3 dBiC, and by about 1 dBiC for 38 GHz. The AR beamwidth of this designed antenna array is 47.21° for 28 GHz and 26.37° for 38 GHz.

The proposed dual band CP single element antenna and its 2×2 array structure are compared to previous mm-wave CP works in Table 2, which demonstrates the proposed antenna's compact size. Simultaneously, the radiation efficiency and gain are extremely high in two mm-wave bands. The other works used many layers or feeding structures to obtain CP, [19] requires metasurface elements to achieve the appropriate reflection coefficient and ARBW. Reference [11] has a lower ARBW, impedance BW, efficiency, and gain than the proposed antenna. The same table contains a comparison of the array to previous 2×2 array works. From this table, it is clear that the majority of them are either linear or have a lower gain or efficiency than the proposed work in this paper, as well as utilizing a bulky structure to provide the CP feature for the antenna array.

V. CONCLUSION

This paper presents a miniaturized single-layer dual-band CP antenna capable of operating at 28 GHz and 38 GHz with high efficiency, good ARBW, and high gain. CMA is utilized in this work to obtain a deep understanding of the physical behavior of the designed antenna, which achieved a gain of 6.73 dBiC at 28 GHz and 5.51 dBiC at 38 GHz, respectively. A 2 × 2 antenna array was designed, analyzed, and fabricated. At 28 GHz, this array achieves a high gain of 12.69 dBiC and at 38 GHz, a high gain of 11.10 dBiC. The developed antenna array is suitable for a variety of 5G applications that require a compact CP array with high gain and efficiency, such as mm-wave mobile communication systems.

REFERENCES

[1] M. Agiwal, A. Roy, and N. Saxena, "Next generation 5G wireless networks: A comprehensive survey," *IEEE Commun. Surveys Tuts.*, vol. 18, no. 3, pp. 1617–1655, 3rd Quart., 2016.

[2] A. I. Sulyman, A. T. Nassar, M. K. Samimi, G. R. Maccartney, T. S. Rappaport, and A. Alsanie, "Radio propagation path loss models for 5G cellular networks in the 28 GHZ and 38 GHZ millimeter-wave bands," *IEEE Commun. Mag.*, vol. 52, no. 9, pp. 78–86, Sep. 2014.

[3] *Engineering the 5G World—Design and Test Insights*, Keysight, Santa Rosa, CA, USA, 2020.

[4] I. Syrytsin, S. Zhang, G. F. Pedersen, and Z. Ying, "User effects on the circular polarization of 5G mobile terminal antennas," *IEEE Trans. Antennas Propag.*, vol. 66, no. 9, pp. 4906–4911, Sep. 2018.

[5] X. L. Bao and M. J. Ammann, "Dual-frequency circularly-polarized patch antenna with compact size and small frequency ratio," *IEEE Trans. Antennas Propag.*, vol. 55, no. 7, pp. 2104–2107, Jul. 2007.

[6] A. Vallecchi and G. B. Gentili, "Design of dual-polarized series-fed microstrip arrays with low losses and high polarization purity," *IEEE Trans. Antennas Propag.*, vol. 53, no. 5, pp. 1791–1798, May 2005.

[7] Nasimuddin, K. P. Esselle, and A. K. Verma, "Wideband circularly polarized stacked microstrip antennas," *IEEE Antennas Wireless Propag. Lett.*, vol. 6, pp. 21–24, 2007.

[8] Y. Zhou, C.-C. Chen, and J. L. Volakis, "Proximity-coupled stacked patch antenna for tri-band GPS applications," in *Proc. IEEE Antennas Propag. Soc. Int. Symp.*, Albuquerque, NM, USA, 2006, pp. 2683–2686.

[9] Y. Lee, S. Ganguly, and R. Mittra, "Multi-band L/sub 5/-capable GPS antenna with reduced backlobes," in *Proc. IEEE Antennas Propag. Soc. Int. Symp.*, vol. 1A. Washington, DC, USA, 2005, pp. 438–441.

[10] B. R. Rao, M. A. Smolinski, C. C. Quach, and E. N. Rosario, "Triple-band GPS trap-loaded inverted L antenna array," *IEEE Microw. Opt. Technol. Lett.*, vol. 38, no. 1, pp. 35–37, Jul. 2003.

[11] H. Aliakbari, A. Abdipour, R. Mirzavand, A. Costanzo, and P. Mousavi, "A single feed dual-band circularly polarized millimeter-wave antenna for 5G communication," in *Proc. 10th Eur. Conf. IEEE Antennas Propag. (EuCAP)*, Davos, Switzerland, 2016. pp. 1–5.

[12] S. Niyamanon, R. Senathong, and C. Phongcharoenpanich, "Dual-frequency circularly polarized truncated square aperture patch antenna with slant strip and L-shaped slot for WLAN applications," *Int. J. Antennas Propag.*, vol. 2018, pp. 1–11, Jul. 2018.

[13] Y.-H. Suh, C. Wang, and K. Chang, "Circularly polarised truncated-corner square patch microstrip rectenna for wireless power transmission," *Electron. Lett.*, vol. 36, no. 7, pp. 600–602, 2000.

[14] P. Mousavi, B. Miners, and O. Basir, "Wideband L-shaped circular polarized monopole slot antenna," *IEEE Antennas Wireless Propag. Lett.*, vol. 9, pp. 822–825, 2010.

[15] S. L. S. Yang, K. F. Lee, A. A. Kishk, and K. M. Luk, "Design of wideband single feed truncated corner microstrip patch antennas for circularly polarized applications," in *Proc. IEEE Antennas Propag. Soc. Int. Symp.*, San Diego, CA, USA, 2008, pp. 1–4.

[16] Z. Chen *et al.*, "Circular polarized 3-D-printed dielectric loaded antenna using inset waveguide-to-dielectric transition for 5G millimeter-wave application," *IEEE Antennas Wireless Propag. Lett.*, vol. 19, pp. 1929–1932, 2020.

[17] Y. Yin, B. Zarghooni, and K. Wu, "Single-layered circularly polarized substrate-integrated waveguide horn antenna array," *IEEE Trans. Antennas Propag.*, vol. 65, no. 11, pp. 6161–6166, Nov. 2017.

[18] N. Hussain, M.-J. Jeong, J. Park, and N. Kim, "A broadband circularly polarized Fabry-Perot resonant antenna using a single-layered PRS for 5G MIMO applications," *IEEE Access*, vol. 7, pp. 42897–42907, 2019.

[19] N. Hussain, M.-J. Jeong, A. Abbas, and N. Kim, "Metasurface-based single-layer wideband circularly polarized MIMO antenna for 5G millimeter-wave systems," *IEEE Access*, vol. 8, pp. 130293–130304, 2020.

[20] C. A. Balanis, *Antenna Theory: Analysis and Design*. Hoboken, NJ, USA: Wiley, 2005.

[21] D. M. Pozar, "Microstrip antennas," *Proc. IEEE*, vol. 80, no. 1, pp. 79–91, Jan. 1992.

[22] M. Nosrati, and N. Tavassolian, "A single feed dual-band, linearly/circularly polarized cross-slot millimeter-wave antenna for future 5G networks," in *Proc. IEEE Int. Symp. Antennas Propag. USNC/URSI Nat. Radio Sci. Meeting*, San Diego, CA, USA, 2017, pp. 2467–2468.

[23] F. I. Alnemr, M. F. Ahmed, and A. A. Shaalan, "Dual-band circularly polarized mobile antenna for millimeter-wave antenna applications," *J. Phys. Conf. Ser.*, vol. 1447, Jan. 2020, Art. no. 12013.

[24] J. Zhu, C.-H. Chu, L. Deng, C. Zhang, Y. Yang, and S. Li, "mm-Wave high gain cavity-backed aperture-coupled patch antenna array," *IEEE Access*, vol. 6, pp. 44050–44058, 2018.

[25] M. M. Kamal *et al.*, "Infinity shell shaped MIMO antenna array for mm-wave 5G applications," *Electronics*, vol. 10, no. 2, p. 165, 2021.

[26] H. Xu, J. Zhou, K. Zhou, Q. Wu, Z. Yu, and W. Hong, "Planar wideband circularly polarized cavity-backed stacked patch antenna array for millimeter-wave applications," *IEEE Trans. Antennas Propag.*, vol. 66, no. 10, pp. 5170–5179, Oct. 2018.

[27] B. Feng, J. Lai, K. L. Chung, T.-Y. Chen, Y. Liu, and C.-Y.-D. Sim, "A compact wideband circularly polarized magneto-electric dipole antenna array for 5G millimeter-wave application," *IEEE Trans. Antennas Propag.*, vol. 68, no. 9, pp. 6838–6843, Sep. 2020.

[28] A. Kesavan, M. Al-Hassan, I. Ben Mabrouk, and T. A. Denidni, "Wideband circular polarized dielectric resonator antenna array for millimeter-wave applications," *Sensors*, vol. 21, no. 11, p. 3614, 2021.

[29] E. A. Abbas, N. Nguyen-Trong, A. T. Mobashsher, and A. M. Abbosh, "Polarization-reconfigurable antenna array for millimeter-wave 5G," *IEEE Access*, vol. 7, pp. 131214–131220, 2019.

[30] M. M. M. Ali and A. Sebak, "Printed RGW circularly polarized differential feeding antenna array for 5G communications," *IEEE Trans. Antennas Propag.*, vol. 67, no. 5, pp. 3151–3160, May 2019.

SAMANEH SADEGHI-MARASHT (Student Member, IEEE) received the M.Sc. degree in telecommunications engineering from the K. N. Toosi University of Technology, Tehran, Iran, in 2015, and the Ph.D. degree from the School of Electrical and Electronic Engineering, University College Dublin (UCD), Dublin, Ireland, in 2022.

From 2017 to 2020, she was a Teaching and a Research Assistant with the Electrical and Electronics Engineering Department, UCD. Her research interests include microwave and millimeter-wave devices modeling and simulation, multiple input multiple output antenna, and 5G applications.

MOHAMMAD S. SHARAWI (Senior Member, IEEE) is a Full Professor of Electrical Engineering with Polytechnique Montréal, Montréal, QC, Canada. He is also a member of the Poly-Grames Research Center, Polytechnique. He was with the King Fahd University of Petroleum and Minerals (KFUPM), Saudi Arabia, from 2009 to 2018. He founded and directed the Antennas and Microwave Structure Design Laboratory, KFUPM. He was a Visiting Professor with the Intelligent Radio Laboratory, Electrical Engineering Department, University of Calgary, Alberta, Canada, during the Summer Fall of 2014. He was a Visiting Research Professor with Oakland University during the summer of 2013. He has more than 350 papers published in refereed journals and international conferences, 11 book chapters (two of which in the Antenna Handbook, 5th edition, McGraw Hill, 2018), one single authored book entitled *Printed MIMO Antenna Engineering* (Artech House, 2014), and the Lead Author of the recent book *Design and Applications of Active Integrated Antennas* (Artech House, 2018). He has 25 issued/granted and 12 pending patents in the U.S. Patent Office. His areas of research include multiband printed multiple-input-multiple-output (MIMO) antenna systems, reconfigurable and active integrated antennas, millimeter-wave antennas, integrated 4g/5g and beyond 5g antenna systems, microwave sensors, applied electromagnetics, and computational methods.

Dr. Sharawi was a recipient of the Abdul Hameed Shoman Foundation Award for Arab researchers for the category of wireless systems in 2020 in addition to various best IEEE conference paper awards. He is serving as the Associate Editor for the IEEE ANTENNAS AND WIRELESS PROPAGATION LETTERS, *IET Microwaves, Antennas and Propagation*, and IEEE OPEN JOURNAL OF ANTENNAS AND PROPAGATION as well as an Area Editor (Antennas and Microwave Devices and Systems) for *Microwave and Optical Technology Letters* (MOP) (Wiley). He is the Specialty Chief Editor for the newly launched *Frontiers in Communications and Networks* for the System and Test-Bed design section. He served on the Technical and organizational program committees as well as organized several special sessions on MIMO antenna systems and architectures in several international conferences, such as EuCAP, IEEE Antennas and Propagation Society (APS), IMWS-5G, APCAP, iWAT among many others for many years. He is the IEEE APS Chair of the Montreal section as well as an active member of the IEEE Member benefits committee leading the initiative of the APS Student Travel Grant. He is also the regional Delegate of the EuRAAP in North America.

ANDING ZHU (Fellow, IEEE) received the Ph.D. degree in electronic engineering from University College Dublin (UCD), Dublin, Ireland, in 2004.

He is currently a Professor with the School of Electrical and Electronic Engineering, UCD. His research interests include high-frequency nonlinear system modeling and device characterization techniques, high-efficiency power amplifier design, wireless transmitter architectures, digital signal processing, and nonlinear system identification algorithms.

Prof. Zhu was a recipient of 2021 IEEE MTT-S Microwave Prize. He is currently a Track Editor of IEEE TRANSACTIONS ON MICROWAVE THEORY AND TECHNIQUES and an Associate Editor of *IEEE Microwave Magazine*. He served as the Secretary of IEEE Microwave Theory and Techniques Society (MTT-S) Administrative Committee (AdCom) in 2018. He is currently an Elected Member of IEEE MTT-S AdCom, the Chair of the Electronic Information Committee, and the Vice Chair of the Marketing and Communications Committee. He served as the Chair of IEEE MTT-S Microwave High-Power Techniques Committee (TC-12) in 2020 and 2021. He is also a member of IEEE Future Directions Committee.